
Article:
Sutherland, G.A. orcid.org/0000-0002-6319-4637, Polak, D., Swainsbury, D.J.K. orcid.org/0000-0002-0754-0363 et al. (11 more authors) (2020) A thermostable protein matrix for spectroscopic analysis of organic semiconductors. Journal of the American Chemical Society, 142 (32). pp. 13898-13907. ISSN 0002-7863

https://doi.org/10.1021/jacs.0c05477

A Thermostable Protein Matrix for Spectroscopic Analysis of Organic Semiconductors

George A. Sutherland†, Daniel Polak‡, David J. K. Swainsbury†, Shuangqing Wang‡, Frank C. Spano§, Dirk B. Auman||, David G. Bossanyi‡, James P. Pidgeon‡, Andrew Hitchcock†, Andrew J. Musser‡, John E. Anthony⊥, P. Leslie Dutton||, Jenny Clark‡ and C. Neil Hunter†*

† Department of Molecular Biology and Biotechnology, University of Sheffield, Sheffield S10 2TN, UK.

‡ Department of Physics and Astronomy, University of Sheffield, Sheffield S3 7RH, UK.

§ Department of Chemistry, Temple University, Philadelphia, PA 19122, USA.

|| Department of Biochemistry and Biophysics, University of Pennsylvania, Philadelphia, PA 19104, USA.

⊥ Department of Chemistry, University of Kentucky, Kentucky 40511, USA.

Semiconductors, protein design, nanoparticles, singlet exciton fission, biomaterials

Abstract

Advances in protein design and engineering have yielded peptide assemblies with enhanced and non-native functionalities. Here, various molecular organic semiconductors (OSCs), with known excitonic up- and down-conversion properties, are attached to a de novo-designed protein, conferring entirely novel functions on the peptide scaffolds. The protein-OSC complexes form similarly-sized, stable, water-soluble nanoparticles that are robust to cryogenic freezing and processing into the solid-state. The peptide matrix enables the formation of protein-OSC-trehalose glasses that fix the proteins in their folded states under oxygen-limited conditions. The encapsulation dramatically enhances the stability of protein-OSC complexes to photodamage, increasing the lifetime of the chromophores from several hours to more than 10 weeks under constant illumination. Comparison of the photophysical properties of astaxanthin aggregates in mixed-solvent systems and proteins shows that the peptide environment does not alter the underlying electronic processes of the incorporated materials, exemplified here by singlet exciton fission followed by separation into weakly-bound, localized triplets. The adaptable protein-based approach lays the foundation for spectroscopic assessment of a broad range of molecular OSCs in aqueous solutions and the solid-state, circumventing the laborious procedure of identifying the experimental conditions necessary for aggregate generation or film formation. The non-native protein functions also raise the prospect of future bio-compatible devices where peptide assemblies could complex with native and non-native systems to generate novel functional materials.

Introduction

Single-junction silicon solar cells are limited by the Shockley-Queisser limit to ~30% power conversion efficiency[1] with technologies aiming to surpass this limit currently under development. One of the more promising schemes is to use energetic up- or down-conversion materials, in conjunction with conventional devices, to capture energy that is either not absorbed or lost as heat within the solar cell.[2-4]

Organic semiconductors (OSCs) offer excitonic up- or down-conversion through the processes of triplet-triplet annihilation (TTA) or singlet exciton fission (SF), respectively.[5] SF is a process where a singlet (spin S=0) exciton converts into a pair of triplet (spin S=1) excitons via a spin-zero triplet-pair state known as ^{1}(TT).[6] The formation of two low-energy triplet excitons from absorption of a single high-energy photon could be harnessed in solar energy devices to overcome thermalization losses.[4, 7, 8] In the reverse process, TTA, a pair of low-energy triplet excitons combines to form a high-energy singlet exciton via the intermediate state ^{1}(TT), allowing up-conversion of energy.[9, 10] However, to date no material has proven ideal and solar up- or down-conversion efficiencies remain low.[4, 9]

In the search for new materials, it is useful to investigate the fundamentals and structure-property characteristics of model SF or TTA systems, and to be able to rapidly analyze any new candidates.[6, 11] Optimally, the study of such processes would occur within a minimal unit, ideally with some control of structure, and should be sufficiently stable to enable optical characterization. The structure of such materials must also be able to withstand processing into the solid-state and characterization at cryogenic temperatures.

A number of studies have described SF in minimal units using covalently-linked molecules or small aggregates formed in solvent mixtures.[12-17] Such structures have resulted in a rapid improvement of our understanding of fundamental SF or TTA processes, such as coupling to charge-transfer states,[18, 19] the role of the solvent environment,[20] vibrations,[21] the formation of long-lived quintet (TT) states,[22, 23] triplet separation[24] and recombination[25]. However, organic synthesis to form covalently-bound supramolecular systems is time-consuming, has only been performed for a

handful of chemical motifs and results in structures that are very different from device-relevant solid-state polycrystalline films. Solvent mixture methods require slow trial-and-error optimization for each molecule with the resulting aggregates often unstable in solution and difficult to transfer to the solid-state. The dramatic effects of temperature on aggregate structure also prevent cryogenic analysis[12]. These difficulties thus preclude the possibility of performing the necessary high throughput detailed physical studies.

Synthetic biology offers the possibility to rapidly generate small multimeric assemblies using de novo-designed artificial protein matrices. Such proteins are free from the evolutionary complexity of natural peptide assemblies and consist of a single polypeptide that self-assembles to form a bundle of four amphipathic helices surrounding a water-excluding cavity.[26-30] This tetrahelical design strategy has generated structures with robustness to chemical and thermal denaturation (melting temperatures >90 °C) that is rarely observed in natural peptides.[31-33] Such proteins have been adapted to facilitate a variety of functions including magnetic-sensing,[34] light-activated redox reactions,[30, 31, 35, 36] peroxide hydrolysis [33] and oxygen transport.[37] Although coordination of cofactors has typically occurred through site-specific ligation to the peptide scaffold, attachment of pigments through hydrophobic interactions has also been suggested.[38-40]

Here, we harness this latter binding regime to attach the carotenoids astaxanthin (AXT), β-carotene (βC) and echinenone (ECH), and show that absorption shifts in all three chromophores arise from identical molecular geometries. The approach is then applied to a wide variety of molecular OSCs, with known excitonic up- or down-conversion properties. Dynamic light-scattering and cryo-electron microscopy are used to investigate the morphology of the OSC-protein complexes, with ultrafast transient absorption spectroscopy demonstrating that the peptide environment does not affect the underlying photophysical properties of the chromophores. The protein-OSC complexes are shown to be robust to cryogenic freezing and processing into the solid-state, where encapsulation in a naturally-occuring optically-clear glass dramatically enhances the photo-stability of the chromophores.

Results and Discussion

Protein characterization. The artificial protein used in this study, herein called 4A, derives from the di-heme binding BT6 protein described previously.[31, 41] In BT6, four positively-charged histidine residues are oriented towards the hydrophobic core of the protein to enable heme attachment. In 4A, all four histidine residues were replaced by hydrophobic alanine residues in order to increase the stability of the peptide scaffold. The amino acid sequences of the two protein variants used in this study are displayed in Table S1 in the Supporting Information.

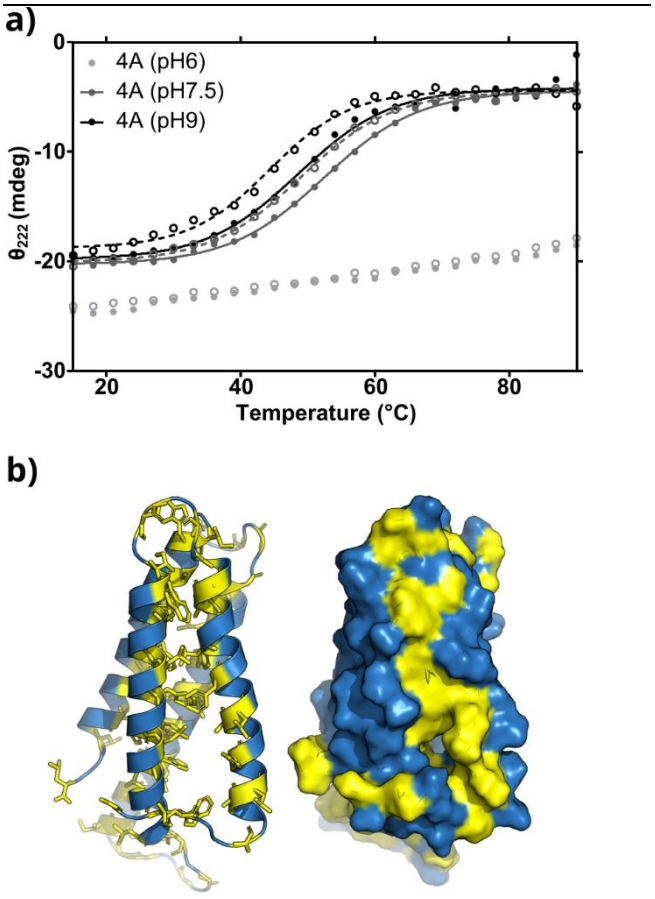

Figure 1. (a) Melting (solid markers) and refolding (open markers) of 4A in aqueous buffer at the indicated pH. Ellipticity was recorded every 1 °C but only every third data point is shown for clarity. Where possible, data points are described by a Boltzmann distribution for melting (solid lines) or refolding (dashed lines). (b) Structural model of the 4A protein, with hydrophobic residues shown in light yellow and hydrophilic residues in blue.

To determine the thermal stability of the proteins, circular dichroism (CD) spectroscopy was used as described previously.[41] CD spectra of BT6 and 4A confirmed that both proteins have typical α-helical character when measured at 15 °C (Figure S1). The presence of α-helical character demonstrates that the proteins fold into their predicted secondary structure. Information about tertiary folding and thermal stability can then be determined by monitoring α-helical ellipticity (at 222 nm) across a reversible temperature gradient, as helical structures will only unfold following collapse of tertiary structure.[42] Melting and refolding curves are described by a Boltzmann distribution where appropriate.

The substitution of four hydrophobic alanine residues resulted in an increase in the thermal stability of 4A, shifting the T_m from 34 °C (BT6, Figure S2) to 49 °C (4A, Figure 1a), when measured at pH 9. At pH 6, the proteins are even more robust; the T_m of BT6 increases to 79 °C (Figure S2) and that of 4A increases beyond the measurable range (>90 °C) (Figure 1a). All melting curves were reversible and showed no

signs of aggregation. These findings suggest that such protein constructs are more durable than most natural counterparts, and should maintain their folded structure at room temperature and during processing.

Structural determination of designed tetrahelical peptides has proved challenging due the repetitive structural motifs, small size and heterogeneous folding.[30, 43, 44] Thus, molecular dynamics (MD) simulated trajectories were used to predict a likely structural conformation of the 4A peptide, using a previously described computational approach.[41] MD trajectories were run for 660 ns with the structure showing convergence over this timescale (Figure S3). The atomic coordinates after 660 ns (Figure 1b) confirm a tetrahelical fold with the majority of the hydrophobic residues (yellow) packing into the protein interior and an elongated hydrophobic cleft exposed on the surface.

Carotenoid-maquette ensembles. To determine whether hydrophobic interactions were sufficient to attach OSCs to the 4A scaffold, the carotenoid astaxanthin (AXT) was incorporated using a solvent-based delivery system. Briefly, AXT was dissolved in dimethyl sulfoxide (DMSO) and mixed 1:4 with buffered aqueous solution containing 4A. An additional experiment was run using the same conditions in the absence of protein. The 4A sample yielded a red, optically-clear solution, while the protein-free solution instantly formed visible precipitant (Figure 2a). Membrane filtration (cellulose acetate, 0.2 μm pore diameter) was sufficient to completely remove all AXT from the protein-free sample, but resulted in little or no change in the AXT content of the 4A sample. The 4A-AXT complex was further purified by anion exchange chromatography (AEC), in a protocol that removed all remaining DMSO and lowered the pH of the buffering solution to 6. The protein elution from the column was red and optically-clear with no visible signs of precipitation.

An identical method (see Supplementary Information for experimental details) was then used to attach the carotenoids echinenone (ECH) and β-carotene (βC) to 4A. All three protein-carotenoid complexes display absorption shifts and changes of vibronic structure relative to monomer dissolved in DMSO, consistent with aggregate formation (Figure 2b-d).[45]

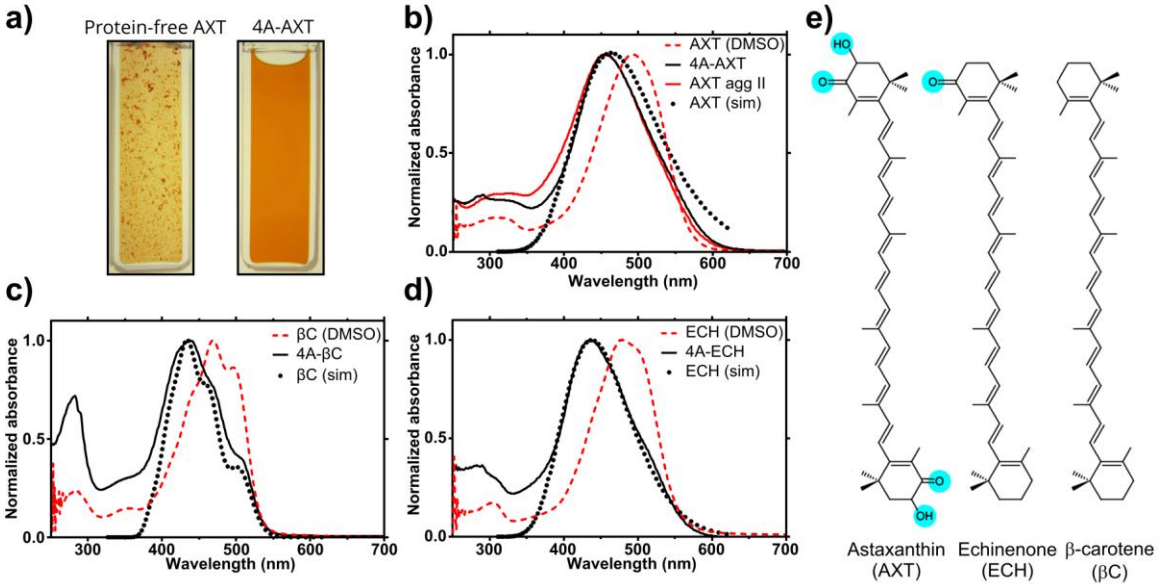

Figure 2. (a) Images of AXT in buffered largely-aqueous solutions (40 mM CHES pH 10, 20% DMSO) without (left) and with (right) 4A. (b-d) Experimentally derived absorption spectra for 4A-carotenoid complexes are shown as black lines, monomeric carotenoid in DMSO as red dashed lines and AXT agg II as a red solid line. The simulated absorption spectra of trimeric assemblies are displayed with black circular markers. All spectra were normalized to the maximum absorbance. (e) Chemical structures of the carotenoids in this study; additional chemical groups, with respect to βC are highlighted in blue.

Analysis of steady-state absorption spectra can be used to describe intermolecular interactions between chromophores, and has been implemented successfully to provide structural information about packing of carotenoid aggregates.[45, 46] This method was used here to simulate the absorption spectrum of a protein-carotenoid ensemble; as accurate modelling requires chromophores with clear vibronic structure, βC was chosen for the modelling. Visual inspection of the spectrum (Figure 2c) shows a relatively weak 0-0 peak with spectral weight shifted to higher energies, indicative of an H-aggregate conformation where excitonic coupling is of the same order of magnitude as the electron-phonon coupling, in this case estimated to be ~0.2 eV.

To analyze the absorption spectrum in more depth, a Holstein Hamiltonian model is applied within the two-particle approximation, following previously reported work.[45, 46] The absorption spectrum of monomeric βC in DMSO was fitted using a standard Franck-Condon progression, assuming one effective vibrational mode couples to the electronic transition. The fit shown in Figure S4 provides values of the 0-0 energy ($\omega_{0\text{-}0}$), the effective vibrational energy (ω_{vib}), the linewidth of the transitions (σ) and the Huang-Rhys parameter (λ^2), which are used in the subsequent modelling.

These values are then used to simulate the absorption spectrum of several βC aggregate arrangements by varying the nearest neighbor coupling (V_{nn}), the angles between

transition dipole moments (φ) and the number of molecules in the aggregate. The simulation that best describes the experimental absorption spectrum of 4A-βC is displayed in Figure 2c (V_{nn}= 1200 cm^{-1}; φ=0.3π; molecule number=3). The majority of the observed absorption appears to arise from a coherent unit of three βC molecules. Simulations using dimers or larger ensembles could not reproduce the measured spectrum with the range of parameters tested (Figures S5, S6 and S7).

Accurately modeling the absorption spectra of ketocarotenoids is more challenging than for βC due to the indistinct vibronic structure that arises from carbonyl groups (Figure 2e), which induce conformational disorder in polar environments.[47] However, the absorption spectrum for 4A-ECH (Figure 2d), can be described by simply increasing σ (the broadening of the vibronic replica) while maintaining other parameters from 4A-βC. An additional red-shift from the 4A-ECH model then describes the spectrum of 4A-AXT (Figure 2b). Thus, the experimentally determined absorption spectra for all three carotenoids are primarily attributable to coherent trimers of equivalent arrangements, with any differences in optical properties arising from the electronic constitution of the chromophores, rather than coupling effects.

Transient absorption spectroscopy of 4A-AXT ensembles. In order to investigate the impact of the peptide environment on the underlying excitonic processes of the bound chromophores, the photophysical properties of 4A-AXT were probed by transient absorption spectroscopy (1 ps-10 μs) and compared with an AXT solution aggregate, herein AXT agg II (red line, Figure 2b), which has been comprehensively characterized in earlier work[12]. Musser and co-workers [12] reported a long-lived (μs) excited-state absorption feature with a ~600 nm maximum in the transient absorption spectra of AXT agg II, which was assigned to triplet states generated via singlet fission. Similar behavior has been reported in other solvent- or membrane-based carotenoid aggregates [48, 49] and in natural light-harvesting assemblies.[50]

To determine whether singlet exciton fission is occurring in the artificial protein-carotenoid ensembles, the transient absorption spectra and dynamics of 4A-AXT are compared with those of AXT agg II and monomeric AXT in DMSO (Figure 3). Near-identical excited-state absorption features are observed in 4A-AXT (greyscale markers) and AXT agg II (red markers) suggesting the underlying photophysics are not altered significantly by the protein. The 4A-AXT spectrum shows negligible evolution over the timescale of the measurement. In addition, AXT agg II and 4A-AXT show similar excited-state dynamics, with absorption features persisting far longer than those of the monomer (red dashed line). As reported previously, these dynamics describe the decay of the triplet excitons generated via singlet fission, with the initial rapid decay (<10 ns) due to geminate triplet-pair recombination and the longer-lived (μs) component due to decay of 'free' (non-interacting or spin-dephased) triplets.[6, 51]. It is perhaps surprising that the S1 and (T..T) excited-state absorption features are so spectrally similar. The nature of this will be discussed at length elsewhere.

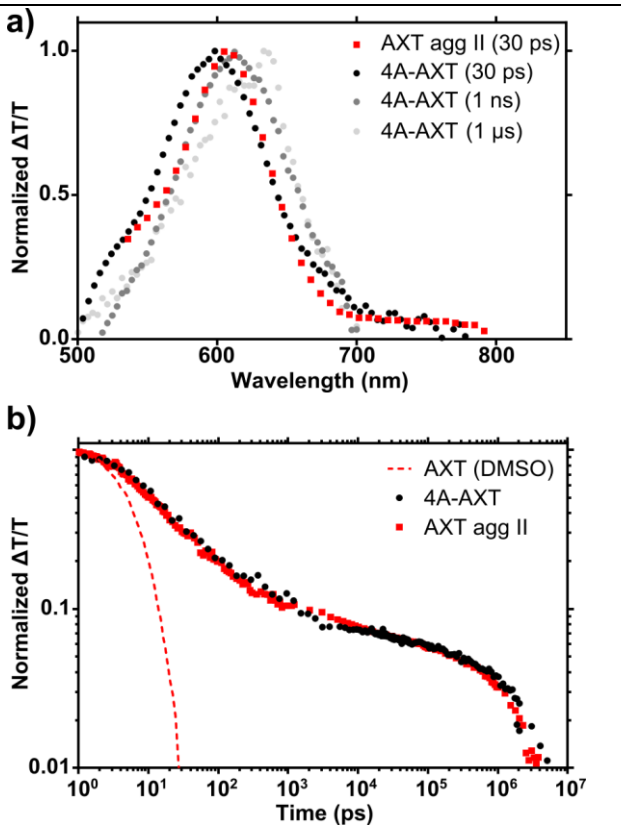

Figure 3. (a) Normalized transient absorption spectra of AXT agg II (red squares) and 4A-AXT (greyscale circles) following the pump-probe delays indicated in parentheses. (b) Transient absorption kinetics of monomeric AXT (red dashed line), AXT agg II (red squares) and 4A-AXT (black circles) are shown as the relative intensity of the 600 nm signal following excitation.

Stability and Morphology of 4A-AXT ensembles. After establishing that the peptide environment does not affect the underlying photophysics of the bound chromophores, the composition and physical properties of the complexes were investigated. As mentioned previously, OSC systems must be robust to cryogenic freezing to enable temperature-dependent assessment of photophysical properties. 4A-AXT complexes in aqueous buffer were flash-frozen in liquid nitrogen and stored for 6 months under standard atmospheric oxygenic conditions at 77 K. Following thawing, only very minor changes were observed in the ground state absorption profile (Figure S8a). The freeze-thaw process was repeated for the 4A-AXT sample numerous times, with no change in spectral character and only 18% reduction in signal after 10 cycles (Figure S8b,c). This suggests that the protein-OSC ensembles are stable to repeated cryogenic cycling and maintain the chromophore arrangement, as any change in molecular packing would be evident from the steady-state absorption.[45]

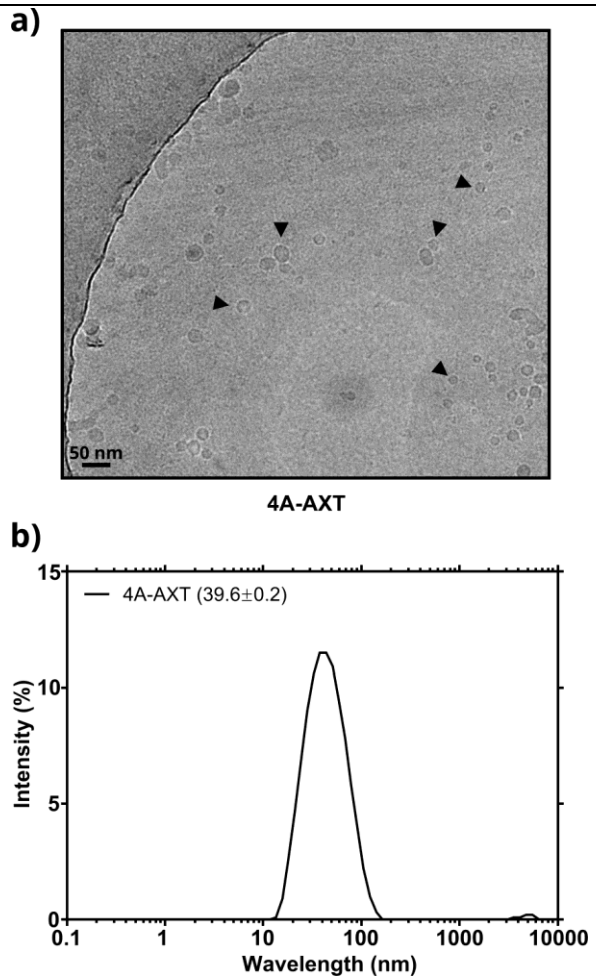

Figure 4. (a) Cryo-EM image of vitreous ice containing 4A-AXT, regions of carbon appear darker grey and vitreous ice lighter. Spherical nanoparticles (highlighted by the black arrows) 10-60 nm in diameter are visible in the vitreous ice. Image representative of 4 experimental repeats. (b) DLS of 4A-OSC complexes in solution with values for the average hydrodynamic diameter (in nm) quoted in parentheses.

Cryo-electron microscopy was used to visualize the morphology of the aqueous 4A-AXT complexes in vitreous ice. Samples revealed circular ensembles 10-60 nm in diameter (Figure 4a, Figure S9) that increase in abundance with increasing protein concentration and are not apparent in samples without AXT. These observations in vitreous ice were compared with dynamic light scattering (DLS) on solutions of 4A-AXT at 550 nm (Zetasizer Nano S90, Malvern Panalytical), revealing an average hydrodynamic diameter of 39.6 ± 0.1 nm (Figure 4b). As the protein itself does not form nanoparticles in the absence of AXT, it is likely that the hydrophobic pi-conjugated molecules induce supramolecular assembly of the peptide units.

Supramolecular association is likely to occur through hydrophobic interactions with non-polar residues in the protein. The requisite amino acids may be permanently available, as suggested by the hydrophobic cleft in Figure 1b, or temporally exposed in response to the presence of hydrophobic cofactors or from the conformationally-flexible (molten-globular) folding state tetrahelical bundle proteins adopt in the absence of coordinating ligands.[31, 43, 44] In order to conformationally constrain the protein scaffold, and sterically restrict access to the internal cavity, two heme *b* molecules were ligated into the hydrophobic core of BT6, as described previously.[41] The di-heme protein was then mixed in solution with AXT, followed by filtration and AEC as described above. This process resulted in little or no trace of the carotenoid in the steady-state absorption spectrum (Figure S10), supporting the notion that AXT binding requires some interaction with the protein core.

Organic semiconductor-protein ensembles. Having demonstrated hydrophobic binding to carotenoids, the concept was adopted for the OSCs shown in Figure 5g, using methods similar to that used for AXT. The present study focuses on OSCs with known excitonic up- or down-conversion, including a triisopropylsilyl-tetracene derivative (T-Tet),[52] a perylene bisimide derivative (EP-PBI),[53] and rubrene.[54, 55-57] Analysis of C8BTBT (2,7-dioctylbenzothienobenzothiophene) was also conducted, which has a fused-ring backbone structure similar to tetracene and rubrene, but is not known to demonstrate excitonic up- or down-conversion.[58]

The absorption spectra in Figure 5a-e show that most protein-OSC complexes display absorption shifts and changes of vibronic structure compared with the monomer dissolved in DMSO, consistent with aggregate formation.[45] An exception is the spectrum of rubrene, which suggests that it either complexes without aggregation or forms an amorphous arrangement with minimal electronic interaction between molecules, similar to reports of the solid-state.[56] For all of the molecules tested, the absorption profile of each protein complex in solution resembles previously reported spectra in solution aggregates or the solid-state (Figure S11).[53, 56, 59, 60]

DLS was used to assess the morphology of each 4A-OSC complex, revealing similar arrangements as 4A-AXT with average hydrodynamic diameters between 63.4 and 90.5 nm (Figure 5f). Polydispersity values for all ensembles were between 0.169 and 0.250. Interestingly, the diameter of the protein-OSC nanoparticles scaled with the bulk size of the molecular structure. This data suggests that the OSC ensembles form spherical supramolecular nanostructures similar to 4A-AXT.

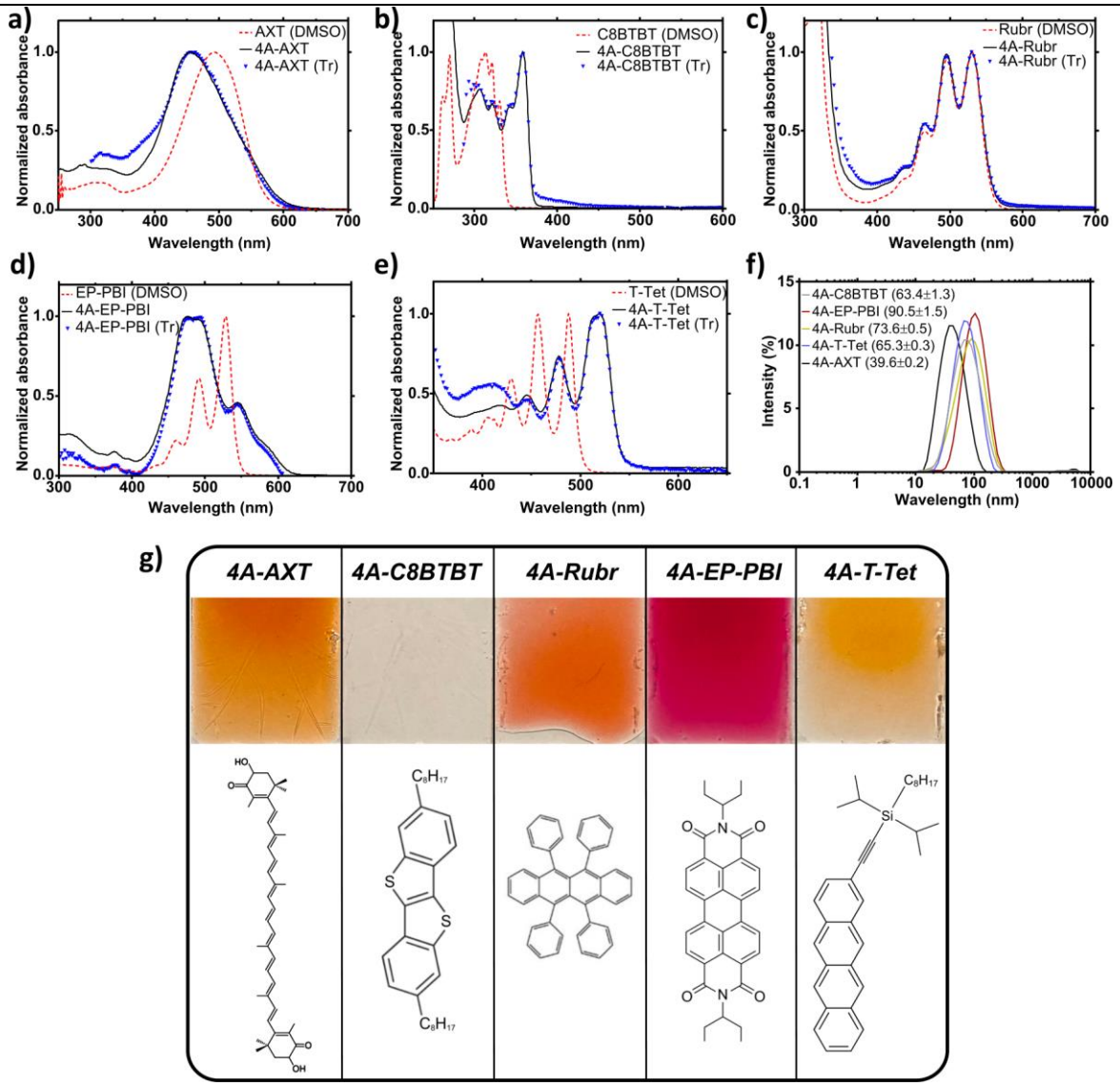

Figure 5. (a-e) Steady-state absorption spectra of several OSCs, solubilized as monomers in DMSO (red dashed lines), aggregates in the aqueous 4A-peptide matrix (black solid lines), or following deposition in trehalose glass (blue triangles). All spectra were normalized to the wavelength maximum >350 nm. (f) DLS of 4A-OSC complexes in solution with values for the average hydrodynamic diameter (in nm) quoted in parentheses. (g) Images of trehalose glasses and the chemical structures of the pigments used in this study.

The protein complexes thus form concentrated, water-based and biocompatible OSC 'inks', using the peptide to solubilize the hydrophobic chromophores. As many photonic applications require solid-state films, optically transparent glasses of the protein-OSC ensembles were made using a trehalose-sucrose matrix. Trehalose is a naturally-occurring sugar produced by plants to protect their macromolecular cellular structures under conditions of extreme drought by fixing proteins in their native conformation.[61] With a glass transition temperature <60 °C, trehalose has been used for optical spectroscopy of protein systems at room temperature, allowing the effects of immobilization and temperature to be distinguished.[62, 63] Protein-OSC ensembles were mixed with an aqueous solution of trehalose and sucrose, deposited on a quartz-substrate and dehydrated by desiccation at room temperature for 4 days in darkness, yielding transparent colored films (Figure 5g). Changes in the ensemble structures upon film formation would be evident in the steady-state absorption spectra as even small changes in molecular packing lead to large spectral shifts.[64, 45] The steady-state absorption spectra in Figure 5a-e show only negligible changes when going from solution (solid black line) to solid-state (blue markers), suggesting that film formation does not alter the structure or photophysical properties of bound chromophores.

Photostability of solid-state glass films. A perpetual challenge for light-active molecules is achieving sufficient photo-stability to withstand intense irradiation. The effects of trehalose encapsulation on photostability were investigated by monitoring the absorption spectra of AXT and T-Tet over time, under constant white-light illumination. Film formation is expected to remove molecular oxygen, most of

the water and conformationally restrict the protein-OSC ensembles, thus increasing the photostability of the coordinated chromophores.

Figures 6a,d show the peak absorbance as a function of time under constant, high white-light illumination (1600 µmol photons s^{-1} m^{-2}) for AXT and T-Tet solution aggregates (red), compared with protein-OSC ensembles in solution (black) and in the solid-state (blue). AXT and T-Tet solution aggregates were made according to the methods described by Musser et al. [12] and Kim et al. [59] respectively.

The peptide matrix does little to prevent photo-oxidative damage in solution, with similar half-life values under illumination, compared to solution aggregates (<8 h for AXT and <5 min for T-Tet). The trehalose films, however, led to dramatic increases in stability over the timescale of the experiments (48 h for AXT, 60 min for T-Tet, Figure S12). Longer exposure under weaker illumination (200 µmol photons s^{-1} m^{-2}) shows that T-Tet absorption is still observed after 9 days (Figure 6b,e), and remarkably, minimal decay in AXT absorption is evident after 70 days (Figure 6c,f).

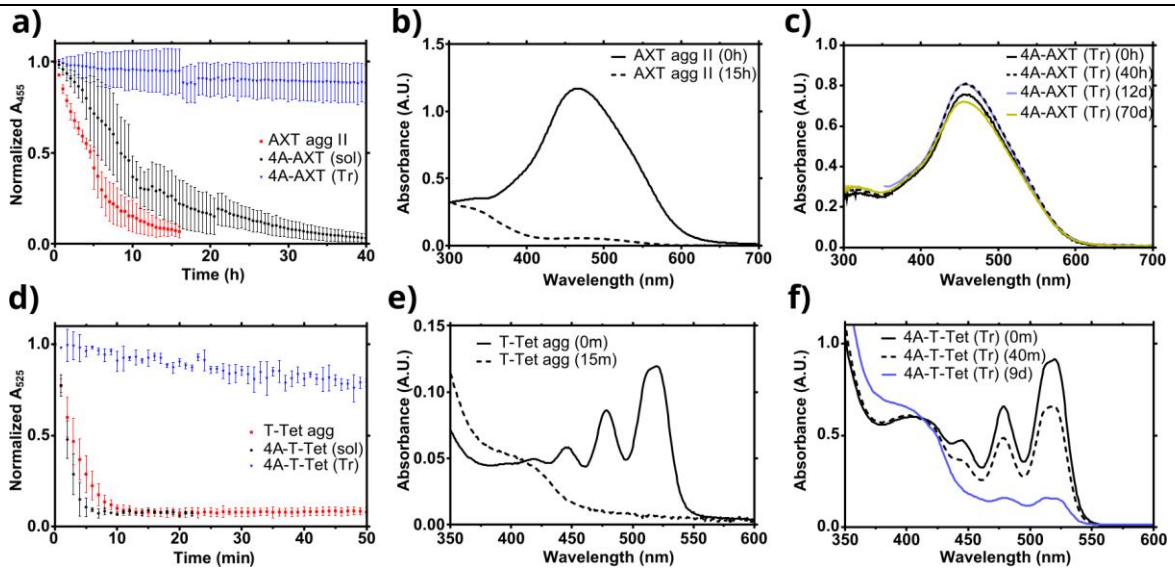

Figure 6. Photostability of OSCs. Photo-oxidative decay of AXT (a) and T-Tet (d) complexed with 4A in solution (black) and following deposition in trehalose glass (blue); AXT agg II and T-Tet agg in mixed solvent systems are shown in red. Data representative of 3 experimental replicates and normalized to the absorbance maxima quoted at 0 min illumination. Absorption spectra of AXT and T-Tet in mixed solvent systems (b, e) and in trehalose glass (c, f) at the time points indicated in the figure legends

Discussion

We have presented the first example of a designed protein construct tailored for the study of excitonic up- and down-conversion materials. The simple design principles in the peptide scaffold enabled attachment of a range of chemical structures using almost identical experimental conditions, thus demonstrating the broad applicability of the protein-based approach.

Although the finding that hydrophobic molecules could be attached to de novo designed tetrahelical peptides is in agreement with previous suggestions, [38-40] the cofactor-induced supramolecular assembly of the 4A complexes was not predicted. While sample heterogeneity precludes atomic-level structural information, constraints on the physical properties of the protein-molecule ensembles can be provided from the observations above. (1) Each OSC becomes highly water-soluble when associated with the proteins, suggesting that the peptides shield the chromophores from polar solvents; (2) the protein-OSC ensembles form circular structures of 30-90 nm diameter, indicating that multiple proteins associate to form the supramolecular architecture; (3) the formation of the ensemble requires some conformational flexibility, allowing the chromophores to associate with the hydrophobic core of the protein; (4) despite this flexibility, the 4A protein displays T_m values above 90 °C; (5) the protein nanoparticles are highly robust to thermal cycling and maintain their photophysical characteristics following solid-state film formation; (6) the carotenoid absorption spectrum is very well described as originating from trimers.

These characteristics of protein-OSCs form the basis for the scheme displayed in Figure S13, in which several interspersed 4A proteins are bound together by chromophore units, visualized here as trimers consistent with the analysis in Figure 2. The notion that individual semiconductor aggregate units intersperse between 4A proteins may also explain the observation that more bulky molecules result in supramolecular structures with larger hydrodynamic radii.

The protein-complexes therefore provide minimal units to study the photophysical properties of OSCs in solution and in the solid-state, with structural information about chromophore packing inferred from spectral modelling, as demonstrated here for three different carotenoids. Although the wide specificity of the simple protein design was necessary to demonstrate applicability to the range of OSCs in this study, more targeted design strategies would result in greater specificity and could enable spatial control of chromophore packing; allowing relationships between pigment arrangement and electronic properties to be deline-

ated. This could be achieved using the plethora of computational and empirical protein design tools available, particularly in silico predictions for ligand binding.[30, 65, 66]

The attachment of OSCs to the peptide scaffolds confers entirely non-native functionality to the proteins. Such biocompatible excitonic up- or down-converting materials could complex with native or non-native biological systems, for example, enhancing the spectral range available to light-harvesting complexes. Protein-mediated up-conversion could be harnessed for biomedical applications by converting highly penetrating low-energy light, generating deleterious photochemical reactions at sites of interest, such as cancer, taking precedent from similar de novo-designed scaffolds used as artificial blood.[67, 68] The protein can additionally be adapted to bind to glass or metallic surfaces, enabling direct patterning of molecular aggregates and the possibility of exploring strong light-matter interactions in well-defined molecular systems.[69, 70]

Conclusion

Thermostable artificial proteins were shown to bind a variety of structurally distinct OSCs, through hydrophobic interactions alone. The proteins were shown to adopt circular supramolecular structures upon binding chromophores, tens of nanometers in diameter. The molecular packing of three carotenoids in the protein nanoparticles was shown to originate from similar chromophore arrangements, which remained robust to cryogenic freezing and deposition into the solid-state. Encapsulation of 4A-OSC complexes in trehalose glass dramatically enhanced the lifetime of the chromophores, giving highly photosensitive molecules – such as T-Tet – sufficient stability for optical assessment, and other semiconductors lifetimes more appropriate for operational use (>10 weeks for AXT). Importantly, the non-specific attachment of chromophore aggregates to the peptide scaffolds did not interfere with the underlying electronic processes of the materials. The work demonstrated here paves the way for future spectroscopic studies on the molecule classes above and will readily extend to other chromophores of interest, particularly compounds with poor stability and those that are not readily processed into the solid-state or solution aggregates.

ASSOCIATED CONTENT

Supporting Information.
Supplementary data and experimental procedures are located in the supporting information (PDF). This material is available free of charge via the Internet at http://pubs.acs.org

AUTHOR INFORMATION

Corresponding Author

*Prof. C. N. Hunter, Department of Molecular Biology and Biotechnology, University of Sheffield, Sheffield S10 2TN, UK.
E-mail: c.n.hunter@sheffield.ac.uk.

Present Addresses

A. J. Musser, Department of Chemistry and Chemical Biology, Cornell University, Ithaca, NY 14853, USA.
D. Polak, School of Chemistry, University of Bristol, Bristol BS8 1TS.
D. B. Auman, Institutionen för biokemi och biofysik, Stockholm 10691, Sweden

Notes

The authors declare no competing financial interests.

ACKNOWLEDGMENT

G.A.S., S.W., J.C. and C.N.H. acknowledge the Engineering and Physical Sciences Research Council (EPSRC) grant EP/S002103/1. D.P. was funded by Faculty of Science Studentships from The University of Sheffield. D.J.K.S., A.H. and C.N.H. were supported by research grant BB/M000265/1 from the Biotechnology and Biological Sciences Research Council (UK). A.H. also acknowledges support from a Royal Society University Research Fellowship, award number URF\R1\191548. C.N.H. also acknowledges European Research Council Synergy Award 854126. D.B.A. was supported by National Institutes of Health Graduate Fellowship T32 GM008275, the Structural Biology & Molecular Biophysics Training Program. A.J.M. would like to acknowledge EPSRC grant EP/M025330/1. F.C.S was supported by the National Science Foundation (DMR-1810838). J.A. was supported by NSF CHE 1609974. Spectroscopic work was supported by the Lord Porter Laser Facility (EP/R042802/1, EP/L022613/1).

REFERENCES

(1) Shockley, W.; Queisser, H. J. Detailed Balance Limit of Efficiency of P-n Junction Solar Cells. *J. Appl. Phys.* **1961**, *32* (3), 510–519.

(2) Day, J.; Senthilarasu, S.; Mallick, T. K. Improving Spectral Modification for Applications in Solar Cells: A Review. *Renew. Energy* **2019**, *132*, 186–205.

(3) Tayebjee, M. J. Y.; McCamey, D. R.; Schmidt, T. W. Beyond Shockley–Queisser: Molecular Approaches to High-Efficiency Photovoltaics. *J. Phys. Chem. Lett.* **2015**, *6* (12), 2367–2378.

(4) Rao, A.; Friend, R. H. Harnessing Singlet Exciton Fission to Break the Shockley–Queisser Limit. *Nat. Rev. Mater.* **2017**, *2* (17063), 1–12.

(5) Smith, M. B.; Michl, J. Recent Advances in Singlet Fission. *Annu. Rev. Phys. Chem.* **2013**, *64* (1), 361–386.

(6) Musser, A. J.; Clark, J. Triplet-Pair States in Organic Semiconductors. *Annu. Rev. Phys. Chem.* **2019**, *70* (1), 323–351.

(7) Dexter, D. L. Two Ideas on Energy Transfer Phenomena: Ion-Pair Effects Involving the OH Stretching Mode, and Sensitization of Photovoltaic Cells. *J. Lumin.* **1979**, *19*, 779–784.

(8) Hanna, M. C.; Nozik, A. J. Solar Conversion Efficiency of Photovoltaic and Photoelectrolysis Cells with Carrier Multiplication Absorbers. *J. Appl. Phys.* **2006**, *100* (7), No. 074510.

(9) Frazer, L.; Gallaher, J. K.; Schmidt, T. W. Optimizing the Efficiency of Solar Photon Upconversion. *ACS Energy Lett.* **2017**, *2* (6), 1346–1354.

(10) Bossanyi, D. G.; Matthiesen, M.; Wang, S.; Smith, J. A.; Kilbride, R. C.; Shipp, J. D.; Holland, E.; Anthony, J. E.; Zaumseil, J.; Musser, A. J.; Clark, J. Emissive spin-0 biexcitons are a direct product of triplet-triplet annihilation. *Nat. Chem.* **2020** (under review)

(11) Sanders, S. N.; Pun, A. B.; Parenti, K. R.; Kumarasamy, E.; Yablon, L. M.; Sfeir, M. Y.; Campos, L. M. Understanding the Bound Triplet-Pair State in Singlet Fission. *Chem* **2019**, *5* (8), 1988–2005.

(12) Musser, A. J.; Maiuri, M.; Brida, D.; Cerullo, G.; Friend, R. H.; Clark, J. The Nature of Singlet Exciton Fission in Carotenoid Aggregates. *J. Am. Chem. Soc.* **2015**, *137* (15), 5130–5139.

(13) Sanders, S. N.; Kumarasamy, E.; Pun, A. B.; Trinh, M. T.; Choi, B.; Xia, J.; Taffet, E. J.; Low, J. Z.; Miller, J. R.; Roy, X.; Zhu, X.-Y.; Steigerwald, M. L.; Sfeir, M. Y.; Campos, L.M. Quantitative Intramolecular Singlet Fission in Bipentacenes. *J. Am. Chem. Soc.* **2015**, *137* (28), 8965–8972.

(14) Korovina, N. V.; Das, S.; Nett, Z.; Feng, X.; Joy, J.; Haiges, R.; Krylov, A. I.; Bradforth, S. E.; Thompson, M. E. Singlet Fission in a Covalently Linked Cofacial Alkynyltetracene Dimer. *J. Am. Chem. Soc.* **2016**, *138* (2), 617–627.

(15) Sanders, S. N.; Kumarasamy, E.; Pun, A. B.; Steigerwald, M. L.; Sfeir, M. Y.; Campos, L. M. Intramolecular Singlet Fission in Oligoacene Heterodimers. *Angew. Chemie* **2016**, *128* (10), 3434–3438.

(16) Liu, H.; Wang, R.; Shen, L.; Xu, Y.; Xiao, M.; Zhang, C.; Li, X. A Covalently Linked Tetracene Trimer: Synthesis and Singlet Exciton Fission Property. *Org. Lett.* **2017**, *19* (3), 580–583.

(17) Piland, G. B.; Bardeen, C. J. How Morphology Affects Singlet Fission in Crystalline Tetracene. *J. Phys. Chem. Lett.* **2015**, *6* (10), 1841–1846.

(18) Lukman, S.; Chen, K.; Hodgkiss, J. M.; Turban, D. H. P.; Hine, N. D. M.; Dong, S.; Wu, J.; Greenham, N. C.; Musser, A. J. Tuning the Role of Charge-Transfer States in Intramolecular Singlet Exciton Fission through Side-Group Engineering. *Nat. Commun.* **2016**, *7*, 1–13.

(19) Margulies, E. A.; Miller, C. E.; Wu, Y.; Ma, L.; Schatz, G. C.; Young, R. M.; Wasielewski, M. R. Enabling Singlet Fission by Controlling Intramolecular Charge Transfer in π-Stacked Covalent Terrylenediimide Dimers. *Nat. Chem.* **2016**, *8* (12), 1120–1125.

(20) Lukman, S.; Musser, A. J.; Chen, K.; Athanasopoulos, S.; Yong, C. K.; Zeng, Z.; Ye, Q.; Chi, C.; Hodgkiss, J. M.; Wu, J.; Friend R. H.; Greenham, N. C. Tuneable Singlet Exciton Fission and Triplet-Triplet Annihilation in an Orthogonal Pentacene Dimer. *Adv. Funct. Mater.* **2015**, *25* (34), 5452–5461.

(21) Fuemmeler, E. G.; Sanders, S. N.; Pun, A. B.; Kumarasamy, E.; Zeng, T.; Miyata, K.; Steigerwald, M. L.; Zhu, X.-Y.; Sfeir, M. Y.; Campos, L. M.; Ananth, N. A Direct Mechanism of Ultrafast Intramolecular Singlet Fission in Pentacene Dimers. *ACS Cent. Sci.* **2016**, *2* (5), 316–324.

(22) Tayebjee, M. J. Y.; Sanders, S. N.; Kumarasamy, E.; Campos, L. M.; Sfeir, M. Y.; McCamey, D. R. Quintet Multiexciton Dynamics in Singlet Fission. *Nat. Phys.* **2017**, *13* (2), 182–188.

(23) Chen, M.; Krzyaniak, M. D.; Nelson, J. N.; Bae, Y. J.; Harvey, S. M.; Schaller, R. D.; Young, R. M.; Wasielewski, M. R. Quintet-Triplet Mixing Determines the Fate of the Multiexciton State Produced by Singlet Fission in a Terrylenediimide Dimer at Room Temperature. *Proc. Natl. Acad. Sci.* **2019**, *116* (17), 8178–8183.

(24) Korovina, N. V.; Chang, C. H.; Johnson, J. C. Spatial Separation of Triplet Excitons Drives Endothermic Singlet Fission. *Nat. Chem.* **2020**, *12* (4), 391–398.

(25) Pun, A. B.; Sanders, S. N.; Sfeir, M. Y.; Campos, L. M.; Congreve, D. N. Annihilator Dimers Enhance Triplet Fusion Upconversion. *Chem. Sci.* **2019**, *10* (14), 3969–3975.

(26) DeGrado, W. F.; Wasserman, Z. R.; Lear, J. D. Protein Design, a Minimalist Approach. *Science* **1989**, *243* (4891), 622–628.

(27) Robertson, D. E.; Farid, R. S.; Moser, C. C.; Urbauer, J. L.; Mulholland, S. E.; Pidikiti, R.; Lear, J. D.; Wand, A. J.; DeGrado, W. F.; Dutton, P. L. Design and Synthesis of Multi-Haem Proteins. *Nature* **1994**, *368*, 425–432.

(28) Edelman, G. M.; Gally, J. A. Degeneracy and Complexity in Biological Systems. *Proc. Natl. Acad. Sci. U. S. A.* **2001**, *98* (24), 13763–13768.

(29) Dutton, P. L.; Moser, C. C. Engineering Enzymes. *Faraday Discuss.* **2011**, *148*, 443–448.

(30) Moser, C. C.; Sheehan, M. M.; Ennist, N. M.; Kodali, G.; Bialas, C.; Englander, M. T.; Discher, B. M.; Dutton, P. L. De Novo Construction of Redox Active Proteins. In *Methods in Enzymology*; 2016; Vol. 580, pp 365–388.

(31) Farid, T. A.; Kodali, G.; Solomon, L. A.; Lichtenstein, B. R.; Sheehan, M. M.; Fry, B. A.; Bialas, C.; Ennist, N. M.; Siedlecki, J. A.; Zhao, Z.; Stetz, M. A.; Valentine, K. G.; Anderson, J. L. R.; Wand, A. J.; Discher, B. M.; Moser, C. C.; Dutton, P. L. Elementary Tetrahelical Protein Design for Diverse Oxidoreductase Functions. *Nat. Chem. Biol.* **2013**, *9* (12), 826–833.

(32) Huang, P. S.; Oberdorfer, G.; Xu, C.; Pei, X. Y.; Nannenga, B. L.; Rogers, J. M.; DiMaio, F.; Gonen, T.; Luisi, B.; Baker, D. High Thermodynamic Stability of Parametrically Designed Helical Bundles. *Science* **2014**, *346* (6208), 481–485.

(33) Watkins, D. W.; Jenkins, J. M. X.; Grayson, K. J.; Wood, N.; Steventon, J. W.; Le Vay, K. K.; Goodwin, M. I.; Mullen, A. S.; Bailey, H. J.; Crump, M. P.; MacMillan, F.; Mulholland, A. J.; Cameron, G.; Sessions, R. B.; Mann, S.; Anderson, J. L. R. Construction and in Vivo Assembly of a Catalytically Proficient and Hyperthermostable de Novo Enzyme. *Nat. Commun.* **2017**, *8* (1), 1–9.

(34) Bialas, C.; Jarocha, L. E.; Henbest, K. B.; Zollitsch, T. M.; Kodali, G.; Timmel, C. R.; Mackenzie, S. R.; Dutton, P. L.; Moser, C. C.; Hore, P. J. Engineering an Artificial Flavoprotein Magnetosensor. *J. Am. Chem. Soc.* **2016**, *138* (51), 16584–16587.

(35) Mancini, J. A.; Kodali, G.; Jiang, J.; Reddy, K. R.; Lindsey, J. S.; Bryant, D. A.; Dutton, P. L.; Moser, C. C. Multi-Step Excitation Energy Transfer Engineered in Genetic Fusions of Natural and Synthetic Light-Harvesting Proteins. *J. R. Soc. Interface* **2017**, *14* (127), 20160896.

(36) Kodali, G.; Mancini, J. A.; Solomon, L. A.; Episova, T. V; Roach, N.; Hobbs, C. J.; Wagner, P.; Mass, O. A.; Aravindu, K.; Barnsley, J. E.; Gordon, K. C.; Officer, D. L.; Dutton, P. l.; Moser, C. C. Design and Engineering of Water-Soluble Light-Harvesting Protein Maquettes. *Chem Sci* **2017**, *8* (1), 316–324.

(37) Koder, R. L.; Anderson, J. L. R.; Solomon, L. A.; Reddy, K. S.; Moser, C. C.; Dutton, P. L. Design and Engineering of an O2 Transport Protein. *Nature* **2009**, *458* (7236), 305–309.

(38) Solomon, L. A.; Kodali, G.; Moser, C. C.; Dutton, P. L. Engineering the Assembly of Heme Cofactors in Man-Made Proteins. *J. Am. Chem. Soc.* **2014**, *136* (8), 3192–3199.

(39) Moser, C. C.; Ennist, N. M.; Mancini, J. A.; Dutton, P. L. Making Maquette Models of Bioenergetic Structures. In *Mechanisms of Primary Energy Transduction in Biology*, 1st Edition; M. Wikström, Eds.; Chemical Biology 5; The Royal Society of Chemistry: London, UK, 2017; pp 1–24.

(40) Mancini, J. A.; Sheehan, M.; Kodali, G.; Chow, B. Y.; Bryant, D. A.; Dutton, P. L.; Moser, C. C. De Novo Synthetic Biliprotein Design, Assembly and Excitation Energy Transfer. *J. R. Soc. Interface* **2018**, *15* (141), 20180021.

(41) Sutherland, G. A.; Grayson, K. J.; Adams, N. B. P.; Mermans, D. M. J.; Jones, A. S.; Robertson, A. J.; Auman, D. B.; Brindley, A. A.; Sterpone, F.; Tuffery, P.; Derreumaux, P.; Dutton, P. L.; Robinson, C.; Hitchcock, A.; Hunter, C. N. Probing the Quality Control Mechanism of the Escherichia Coli Twin-Arginine Translocase with Folding Variants of a de Novo– Designed Heme Protein. *J. Biol. Chem.* **2018**, *293* (18), 6672–6681.

(42) Greenfield, N. J. Using Circular Dichroism Collected as a Function of Temperature to Determine the Thermodynamics of Protein Unfolding and Binding Interactions. *Nat. Protoc.* **2006**, *1* (6), 2527–2535.

(43) Gibney, B. R.; Rabanal, F.; Skalicky, J. J.; Wand, A. J.; Dutton, P. L. Design of a Unique Protein Scaffold for Maquettes. *J. Am. Chem. Soc.* **1997**, *119* (9), 2323–2324.

(44) Huang, S. S.; Gibney, B. R.; Stayrook, S. E.; Dutton, L. P.; Lewis, M. X-Ray Structure of a Maquette Scaffold. *J. Mol. Biol.* **2003**, *326* (4), 1219–1225.

(45) Hestand, N. J.; Spano, F. C. Expanded Theory of H- and J-Molecular Aggregates: The Effects of Vibronic Coupling and Intermolecular Charge Transfer. *Chem. Rev.* **2018**, *118* (15), 7069–7163.

(46) Spano, F. C. Analysis of the UV/Vis and CD Spectral Line Shapes of Carotenoid Assemblies: Spectral Signatures of Chiral H-Aggregates. *J. Am. Chem. Soc.* **2009**, *131* (12), 4267–4278.

(47) Spano, F. C.; Silva, C. H- and J-Aggregate Behavior in Polymeric Semiconductors. *Annu. Rev. Phys. Chem.* **2014**, *65* (1), 477–500.

(48) Billsten, H. H.; Sundström, V.; Polívka, T. Self-Assembled Aggregates of the Carotenoid Zeaxanthin: Time-Resolved Study of Excited States. *J. Phys. Chem. A* **2005**, *109* (8), 1521–1529.

(49) Wang, C.; Tauber, M. J. High-Yield Singlet Fission in a Zeaxanthin Aggregate Observed by Picosecond Resonance Raman Spectroscopy. *J. Am. Chem. Soc.* **2010**, *132* (40), 13988–13991.

(50) Yu, J.; Fu, L. M.; Yu, L. J.; Shi, Y.; Wang, P.; Wang-Otomo, Z. Y.; Zhang, J. P. Carotenoid Singlet Fission Reactions in Bacterial

Light Harvesting Complexes As Revealed by Triplet Excitation Profiles. *J. Am. Chem. Soc.* **2017**, *139* (44), 15984–15993.

(51) Musser, A. J.; Al-Hashimi, M.; Heeney, M.; Clark, J. Heavy-Atom Effects on Intramolecular Singlet Fission in a Conjugated Polymer. *J. Chem. Phys.* **2019**, *151* (4), 0044902.

(52) Anthony, J. E. The Larger Acenes: Versatile Organic Semiconductors. *Angew. Chemie - Int. Ed.* **2008**, *47* (3), 452–483.

(53) Kennehan, E. R.; Grieco, C.; Brigeman, A. N.; Doucette, G. S.; Rimshaw, A.; Bisgaier, K.; Giebink, N. C.; Asbury, J. B. Using Molecular Vibrations to Probe Exciton Delocalization in Films of Perylene Diimides with Ultrafast Mid-IR Spectroscopy. *Phys. Chem. Chem. Phys.* **2017**, *19* (36), 24829–24839.

(54) Schulze, T. F.; Schmidt, T. W. Photochemical Upconversion: Present Status and Prospects for Its Application to Solar Energy Conversion. *Energy Environ. Sci.* **2015**, *8* (1), 103–125.

(55) Pandey, A. K.; Nunzi, J. M. Upconversion Injection in Rubrene/Perylene-Diimide-Heterostructure Electroluminescent Diodes. *Appl. Phys. Lett.* **2007**, *90* (26), 1–4.

(56) Hodges, M. P. P.; Grell, M.; Morley, N. A.; Allwood, D. A. Wide Field Magnetic Luminescence Imaging. *Adv. Funct. Mater.* **2017**, *27* (31), 1–7.

(57) Gray, V.; Moth-Poulsen, K.; Albinsson, B.; Abrahamsson, M. Towards Efficient Solid-State Triplet–Triplet Annihilation Based Photon Upconversion: Supramolecular, Macromolecular and Self-Assembled Systems. *Coord. Chem. Rev.* **2018**, *362*, 54–71.

(58) Yuan, Y.; Giri, G.; Ayzner, A. L.; Zoombelt, A. P.; Mannsfeld, S. C. B.; Chen, J.; Nordlund, D.; Toney, M. F.; Huang, J.; Bao, Z. Ultra-High Mobility Transparent Organic Thin Film Transistors Grown by an off-Centre Spin-Coating Method. *Nat. Commun.* **2014**, *5*, 1–9.

(59) Kim, H. Y.; Bjorklund, T. G.; Lim, S.-H.; Bardeen, C. J. Spectroscopic and Photocatalytic Properties of Organic Tetracene Nanoparticles in Aqueous Solution. *Langmuir* **2003**, *19* (9), 3941–3946.

(60) Keum, C.-M.; Liu, S.; Al-Shadeedi, A.; Kaphle, V.; Callens, M. K.; Han, L.; Neyts, K.; Zhao, H.; Gather, M. C.; Bunge, S. D.; Twieg, R. J.; Jakli, A.; Lüssem, B. Tuning Charge Carrier Transport and Optical Birefringence in Liquid-Crystalline Thin Films: A New Design Space for Organic Light-Emitting Diodes. *Sci. Rep.* **2018**, *8* (1), 699.

(61) Sampedro, J. G.; Uribe, S. Trehalose-Enzyme Interactions Result in Structure Stabilization and Activity Inihibition. The Role of Viscosity. *Mol. Cell. Biochem.* **2004**, *256–257* (1–2), 319–327.

(62) Jain, N. K.; Roy, I. Effect of Trehalose on Protein Structure. *Protein Science*. 2009, pp 24–36.

(63) Kurashov, V.; Gorka, M.; Milanovsky, G. E.; Johnson, T. W.; Cherepanov, D. A.; Semenov, A. Y.; Golbeck, J. H. Critical Evaluation of Electron Transfer Kinetics in P700–FA/FB, P700–FX, and P700–A1 Photosystem I Core Complexes in Liquid and in Trehalose Glass. *Biochim. Biophys. Acta - Bioenerg.* **2018**, *1859* (12), 1288–1301.

(64) Musser, A. J.; Rajendran, S. K.; Georgiou, K.; Gai, L.; Grant, R. T.; Shen, Z.; Cavazzini, M.; Ruseckas, A.; Turnbull, G. A.; Samuel, I. D. W.; Clark, J.; Lidzey, D. G. Intermolecular States in Organic Dye Dispersions: Excimers: Vs. Aggregates. *J. Mater. Chem. C* **2017**, *5* (33), 8380–8389.

(65) Morris, G. M.; Huey, R.; Lindstrom, W.; Sanner, M. F.; Belew, R. K.; Goodsell, D. S.; Olson, A. J. AutoDock4 and AutoDockTools4: Automated Docking with Selective Receptor Flexibility. *J. Comput. Chem.* **2009**, *30* (16), 2785–2791.

(66) Huang, P.-S.; Boyken, S. E.; Baker, D. The Coming of Age of de Novo Protein Design. *Nature* **2016**, *537* (7620), 320–327.

(67) Dutton, P. L. Artificial oxygen transport protein. U. S. Patent 8846619B2, March 4, 2010.

(68) Cheng, L.; Wang, C.; Liu, Z. Upconversion Nanoparticles and Their Composite Nanostructures for Biomedical Imaging and Cancer Therapy. *Nanoscale* **2013**, *5* (1), 23–37.

(69) Tsargorodska, A.; Cartron, M. L.; Vasilev, C.; Kodali, G.; Mass, O. A.; Baumberg, J. J.; Dutton, P. L.; Hunter, C. N.; Törmä, P.; Leggett, G. J. Strong Coupling of Localized Surface Plasmons to Excitons in Light-Harvesting Complexes. *Nano Lett.* **2016**, *16* (11), 6850–6856.

(70) Lishchuk, A.; Vasilev, C.; Johnson, M. P.; Hunter, C. N.; Törmä, P.; Leggett, G. J. Turning the Challenge of Quantum Biology on Its Head: Biological Control of Quantum Optical Systems. *Faraday Discuss.* **2019**, *216*, 57–71.

.

Table of Contents artwork